Geomechanics and Engineering, *Vol. 16, No. 5 (2018) 513-525*
DOI: https://doi.org/10.12989/gae.2018.16.5.513

Analyses of centrifuge modelling for artificially sensitive clay slopes

Dong Soon Park*

K-water Convergence Research Institute, Korea Water Resources Corporation, 125, 1689beon-gil, Yuseong-daero, Yuseong-gu, Daejeon 34045, Republic of Korea

(Received February 21, 2018, Revised September 17, 2018, Accepted September 28, 2018)

Abstract. Slope stability of sensitive clayey soils is particularly important when subjected to strength loss and deformation. Except for progressive failure, for most sensitive and insensitive slopes, it is important to review the feasibility of conventional analysis methods based on peak strength since peak strength governs slope stability before yielding. In this study, as a part of efforts to understand the behavior of sensitive clay slopes, a total of 12 centrifuge tests were performed for artificially sensitive and insensitive clay slopes using San Francisco Bay Mud (PI = 50) and Yolo Loam (PI = 10). In terms of slope stability, the results were analyzed using the updated instability factor (N_I). N_I using equivalent unit weight to cause a failure is in reasonable agreement shown in the Taylor's chart (N_I ~ 5.5). In terms of dynamic deformation, it is shown that two-way sliding is a more accurate approach than conventional one-way sliding. Two-way sliding may relate to diffused shear surfaces. The outcome of this study is contributable to analyzing stability and deformation of steep sensitive clay slopes.

Keywords: sensitive clay; slope stability; sensitivity; cement treated; centrifuge model; limit equilibrium

1. Introduction

Static and dynamic slope stability of sensitive clayey soils is particularly important when subjected to sudden destructuration induced by external loading or earthquakes.

According to the database of recent landslide events in worldwide provided by the Geological Survey of Canada (Couture 2011) and the US Geological Survey (USGS 2015), it is believed that many landslides have occurred in sensitive clay. A typical example of the abrupt collapse of sensitive clay was shown at Saint-Jude, Quebec in Canada, May 2010 (Locat *et al*. 2012). It is also reported that there have been cases of extensive submarine or in-land landslides for the weakly cemented sensitive clay layer (Andersson-Sköld *et al*. 2005, Azizian and Popescu 2005, Crawford 1968, Demers et al. 2014, Geertsema and Torrance 2005, L'Heureux *et al*. 2014, Longva *et al*. 2003, Tappin *et al*. 2003). Quinn *et al*. (2011) reported that some largest recorded landslides in sensitive clays are associated with the earthquakes–e.g., Saint-Jean-Vianney and Shawinigan landslides caused by the 1663 Charlevoix earthquake (Legget and LaSalle 1978, Quinn *et al*. 2011). Deformation can be significantly large if sensitive clay and liquefiable sand/silt layer exist together as seen in the Turnagain Heights landslide, which occurred due to the Alaska earthquake in 1964 (Seed and Wilson 1966, Updike *et al*. 1988).

Sensitive clays can be classified by their sensitivity (S_t; the ratio of the strength in the undisturbed state to that in the remolded state). Classifications of sensitivity are different in different regions. In this study, whether soils are medium sensitive or highly sensitive was determined by the US classification of Holtz and Kovacs (1981).

For sensitive clay during the remolding, most of effective stresses which had been carried by the mineral skeleton are transferred to the pore water. Thus, the main concern for sensitive clay is strength loss and extensive deformation potential due to destructuration and/or dynamic loading. It is therefore beneficial to study the relationship between shear strength, instability of slopes, and resulting displacement.

Recently, significant efforts to develop constitutive models have been made to account for the mechanism of destructuration of sensitive clay in the field of numerical modeling (Dey *et al*. 2016a, Dey *et al*. 2016b, Park and Kutter 2016, Rezania *et al*. 2016, Thakur and Nordal 2005). On the other hand to study this issue, physical modelling can be a useful way particularly in case of challenging sampling and modelling in a repeatable manner. In fact, many researchers have used physical modeling of systems constructed with soft clay to better understand its behavior. The geo-centrifuge has been successfully used due to its ability to reproduce the in-situ strength and stiffness profiles of soft clays. However, few models simulating sensitive clay soils have been performed.

It is very expensive to use undisturbed sensitive clay samples to study behavior of sensitive clay slopes. As an experimental approach to study the behavior of sensitive clay slopes indirectly, a construction technique to create sensitive clay in laboratory was developed using a weak cement mix (Park *et al*. 2014). Using the proposed technique, the instability and deformation of slopes were tested using centrifuge tests for eleven cement-treated artificially sensitive clay slopes and one uncemented clay slope (Park and Kutter 2015).

*Corresponding author, Ph.D.
E-mail: dspark210@gmail.com

http://www.techno-press.org/?journal=gae&subpage=7
ISSN: 2005-307X (Print), 2092-6219 (Online)

According to Park and Kutter (2015), peak shear strength governs the stability and deformation of clay slopes before yielding if the slopes do not fail in a progressive pattern. Therefore, it is important to review the adaptability of conventional analyses methods based on peak strength. In this study, simpler and more practical methods are introduced to explain static stability and dynamic deformation of sensitive clay slopes. Analytical and numerical analyses are accommodated to simulate sensitive clay soil behavior by modifications of traditional methods such as stability factor and limit equilibrium analysis. First, instability factor (N_I), which is a modified form of the traditional stability number (N) (Taylor 1937, 1948) is correlated with the performance of the centrifuge model slope tests. Second, instability and consequential deformation are examined through static and pseudo-static limit equilibrium analysis by using SLOPE/W program (GEO-SLOPE International Ltd 2010). Newly introduced terms of equivalent unit weight (γ_e) and two-way sliding are incorporated with the slope stability and deformation analysis. Some important findings and observations for these approaches are described.

2. Centrifuge modelling

2.1 Program design

Table 1 summarizes different combinations of total 12 centrifuge tests. General layout for centrifuge modelling is shown in the Fig. 1. All detailed information is described in the previously published paper by Park *et al*. (2010) and Park and Kutter (2015). For this reason, in this article, the author intended to address only essential test procedures and description. Out of 12 tests, the four (DSP1-4) were static tests without earthquake shaking to monitor the response of static slope deformation, consolidation features, and failure criteria.

For the testing, the 1-m radius centrifuge at the Center for Geotechnical Modeling at UC Davis was used. The centrifuge was equipped with a new 1-D shaker system (Wilson *et al*. 2010). The advantage of the small centrifuge is the relative ease of operation, providing the ability to conduct a larger number of experiments. Centrifuge testing involves the centrifuge itself, shaker, transparent-wall rigid container, multiple accelerometers, pore pressure transducers, displacement transducers, and associated data acquisition hardware and software. In this research, the similitude laws shown in Garnier *et al.* (2007) were applied to scale a clay slope model in the centrifuge to a full scale prototype.

Note that prototype geometry by centrifuge acceleration should be curved because of radial G-field effect (Park 2014). Radial G-field effect can be one of the biggest concerns when both rotation direction and longitudinal direction of model container coincide with each other, especially in a small centrifuge with a large model. In the test configuration, rotation radius of the centrifuge is about 1.0 m, and the length of the container box is 0.56 m. Thus, a constant radius curved water table in model scale represents a flat water table in the prototype. Linearly constructed

Table 1 Centrifuge test program

Test ID	Test label	Test type	H_i	Target G-level	γ_t	S_u	S_{ur}	S_t
			mm	g	kN/m^3	kPa	kPa	
DSP1	SFBM C5W199T6	Static	100	50	12.6	16.3	2.0	8
DSP2	SFBM C5W249T6	Static	120	50	11.9	5.9	0.5	13
DSP3	SFBM C3W135T9	Static	120	50	13.7	4.0	1.4	3
DSP4	YL C3W47T5	Static	120	50	17.1	84.2	6.8	12
DSP5	YL C3W51T4	Dynamic	120	50	17.0	62.5	4.3	15
DSP6	SFBM C4W214C2	Dynamic	120	50	12.4	3.3	0.4	9
DSP7	SFBM C4W195T2.4	Dynamic	120	50	12.6	4.8	0.5	9
DSP8	SFBM C4W170T7	Dynamic	120	50	12.9	9.8	1.8	5
DSP9	YL C2W51T3	Dynamic	120	50	17.3	18.0	1.8	10
DSP10	SFBM C5W220T1	Dynamic	120	50	12.3	4.5	0.4	11
DSP11	YL C2W55T3	Dynamic	120	50	16.3	12.2	0.6	20
DSP12	Uncemented YL W40	Dynamic	120	50	17.8	10.9	5.1	2

Note: H_i = initial slope height between crest and base (in model scale), γ_t = total unit weight, S_u = undrained peak shear strength, S_{ur} = remolded shear strength

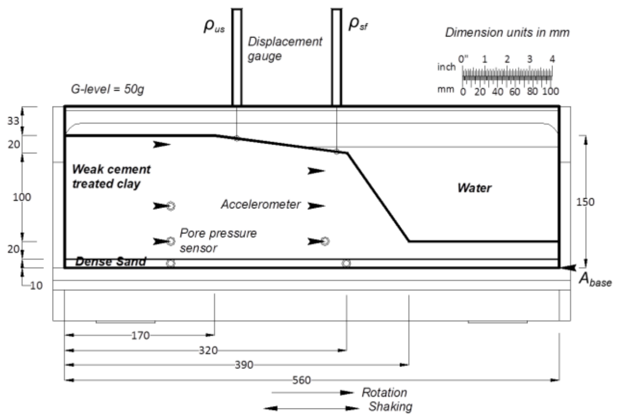

Fig. 1 Typical test design section of sensitive clay slope in a container Note, ρ_{us} = measured settlement on the upslope linear potentiometer, ρ_{sf} = measured settlement on the steep slope side linear potentiometer, A_{base} = accelerometer installed on the rigid base container.

slope geometry in model should be curved hill shape geometry in prototype because of radial G-field. Therefore, converted prototype geometry can be calculated (Fig. 2). The middle portion of up- and down- slopes are almost undistorted, but outer portion of flat surface in model represents significantly sloping ground in prototype.

It is useful to define some notations to characterize features of artificially sensitive clay slope behavior. In this paper, the following terms are defined (Fig. 3).

• Major slip surface: If the slope failure is obviously distinct, it is the same as the rupture surface. If the failure occurs in a more or less diffused manner, it is defined as the locus of deepest major kink points of deformed columns (as visualized using pasta noodles placed in the model during

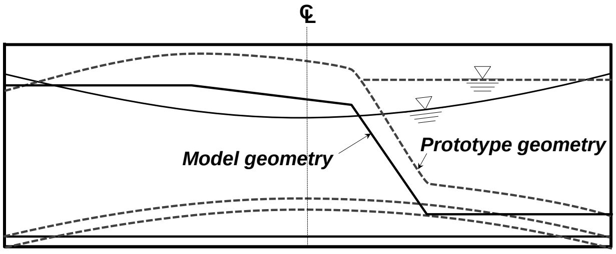

Fig. 2 Estimated prototype geometry due to radial G-field effect

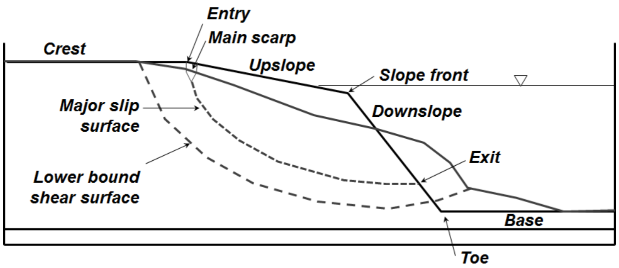

Fig. 3 Glossary of terms used in this study

construction).

• Lower bound shear surface: The deepest shear surface showing the significant shear strain at each depth of column. Here, the significant shear strain means the shear strain of about 100% through the observation of deformed shape of each deformation column. Note that the thickness of pasta noodles was about 2 mm, hence the significant shear strain was the strain to indicate about 2 mm of horizontal displacement.

• Crest: The upper flat portion of soil mass in the model slope.

• Base: The lower flat portion of soil mass in the model slope.

• Upslope: The upper part of slope in a double-sloping ground, denoted as 'us.'

• Downslope: The lower part of slope in a double-sloping ground.

• Slope front: The point where upslope and downslope surfaces meets at, denoted as 'sf.'

2.2 Instability factor

For static and dynamic centrifuge modeling for artificially sensitive clay slopes in this study, one important purpose is to investigate the applicability of simpler analytical approaches using instability factor with an appropriate modification of their original form.

The concept of stability number, N was originated from Taylor's stability chart (1937). Although many updated versions of stability charts have been developed (Baker *et al*. 2006, Duncan and Wright 2005, Gibson and Morgenstern 1962, Janbu 1968, Javankhoshdel and Bathurst 2014, Spencer 1967, Steward *et al*. 2011, Talesnick and Baker 1984), the traditional stability number concept is still similar. Stability number, N for φ = 0 soil (total stress analysis) is defined as

$$N = \frac{c_u}{FS \cdot \gamma H} = \frac{c_m}{\gamma H} \tag{1}$$

where, c_u: undrained strength of soil, FS: factor of safety, γ: unit weight of soil, H: height of slope from the crest to the base, c_m: mobilized shear strength ($c_m = c_u / FS$; factor of safety is regarded as the ratio of shear strength of soil divided by strength being mobilized).

Because the instability of clay slope generally increases with the weight of soil mass as a driving force, the inverse form of stability number can be conceptually convenient to understand how unstable the slope is. Hence, in this study, the "instability factor (N_I)" is defined as

$$N_I = \gamma H / S_u \tag{2}$$

In this definition, γ is the unit weight of soil, $\gamma = \gamma_t$ (total unit weight) above the water level, $\gamma = \gamma'$ (buoyant unit weight) below the water table, and S_u is the undrained strength of soil layer.

As shown in Fig. 4, unit weight should be different above and below the water table because of the curved water table in the centrifuge model. Thus, the equivalent unit weight (γ_e) used to compute instability factor was obtained by calculating weighted average value of total and buoyant unit weights considering each volume relative to the impounded water table (Fig. 4). Then, the instability factor (N_I) can be re-written as

$$N_I = \gamma_e H / S_u \tag{3}$$

In this study, N_I has a different value depending on measured shear strength at different depth. Besides, N_I gradually reduces as slope deformation occurs because of a change of slope height (H) and equivalent unit weight (γ_e). Therefore, it is necessary to define incremental slope height, equivalent unit weight, and corresponding N_I to cause a certain deformation at least for both initial and final geometry. From the measured total settlement (ρ_f) and the final height (H_f), equivalent unit weight and slope height at 5% and 10% settlement of slope height can be linearly approximated. Fig. 4 shows how to calculate equivalent unit weight. Note that γ_t is the total unit weight and γ_b is the buoyant unit weight in Fig. 4.

$$\gamma_{ei} = \frac{\gamma_t \cdot A_{above} + \gamma_b \cdot A_{below}}{A_{above} + A_{below}} \quad \text{for initial undeformed geometry} \tag{4}$$

$$\gamma_{ef} = \frac{\gamma_t \cdot A_{above} + \gamma_b \cdot A_{below}}{A_{above} + A_{below}} \quad \text{for final deformed geometry} \tag{5}$$

$$\gamma_{e,5\%} = \gamma_{ei} - (\gamma_{ei} - \gamma_{ef}) \cdot \frac{\rho_{5\%}}{\rho_f} \tag{6}$$

$$\gamma_{e,10\%} = \gamma_{ei} - (\gamma_{ei} - \gamma_{ef}) \cdot \frac{\rho_{10\%}}{\rho_f} \tag{7}$$

$$H_{5\%} = H_i - (H_i - H_f) \cdot \frac{\rho_{5\%}}{\rho_f} \tag{8}$$

$$H_{10\%} = H_i - (H_i - H_f) \cdot \frac{\rho_{10\%}}{\rho_f} \quad (9)$$

where, γ_{ei} = initial equivalent unit weight for undeformed geometry, γ_{ef} = final equivalent unit weight for deformed geometry, $\gamma_{e,5\%}$ = equivalent unit weight corresponding to the 5% settlement of slope height on the upslope potentiometer, $\gamma_{e,10\%}$ = equivalent unit weight corresponding to the 10% settlement of slope height on the upslope potentiometer, H_i= initial slope height for undeformed geometry, H_f = final slope height for deformed geometry, $H_{5\%}$ = slope height corresponding to the 5% initial slope height, $H_{10\%}$ = slope height corresponding to the 10% initial slope height, ρ_f = final settlement measured on the upslope potentiometer, $\rho_{5\%}$ = 5% upslope settlement with respect to the initial slope height ($\rho_{5\%} = 5\% \cdot H_i$), $\rho_{10\%}$ = 10% upslope settlement with respect to the initial slope height ($\rho_{10\%} = 10\% \cdot H_i$).

To define failure in this study, upslope displacement gauge in Fig. 1 was used because it showed relatively stable and consistent results with visual inspection of shear failure of slope in a general scale.

Based on conventional Taylor (1948)'s stability chart, slopes are unstable if the instability factor reaches 5.5 when there is no restriction of base depth. Note that the later version of Gibson and Morgenstern (1962)'s chart approach may be more appropriate for the analyses of slope stability in terms of the consideration of strength gradient per depth. However, stability number calculation using Gibson and Morgenstern (1962)'s method was not practically appropriate to apply in this study because of non-zero shear strength near the surface and the application of equivalent unit weight (γ_e) considering above and below the water table for the computation of instability factor. Gibson and Morgenstern (1962) assumes zero strength at the surface and single value of proportional constant (for varying strength as a function of depth), and uniform stability number only depending on the angle of slope, which was not applicable in this centrifuge model cases. For limit equilibrium analyses, material strength profile as a function of depth was adopted in this paper. However, single representative shear strength was simply used for the computation of instability factor for comparison purposes.

2.3 Materials

The raw materials used in this research are San Francisco Bay Mud (SFBM) and Yolo Loam (YL). San Francisco Bay Mud is a high plasticity clay (Liquid Limit, LL = 88%, Plasticity Index, PI = 50%, classified as CH in USCS) while Yolo Loam is a low plasticity clay (LL = 29%, PI = 10%, classified as CL in USCS). The typical engineering properties for raw SFBM and YL are shown in Table 2.

Portland Cement Type 1 was chosen as a main additive in this study. There are mainly three variables to construct sensitive clay (as shown in Park *et al.* 2014); cement mix ratio, initial water content, and curing days. For convenience, each term is denoted as "C (%)", "W (%)", and "T (days)". For example, the symbol YL C2W35T5 represents cemented Yolo Loam with 2% cement mixing ratio, 35% initial water content of clay slurry, and a 5 day curing period. Cement mixing ratio is defined as the mass ratio of dry Portland cement (Type 1) with respect to that of mass of soil solids. Initial water content is the water content of slurry soil before cement mixing.

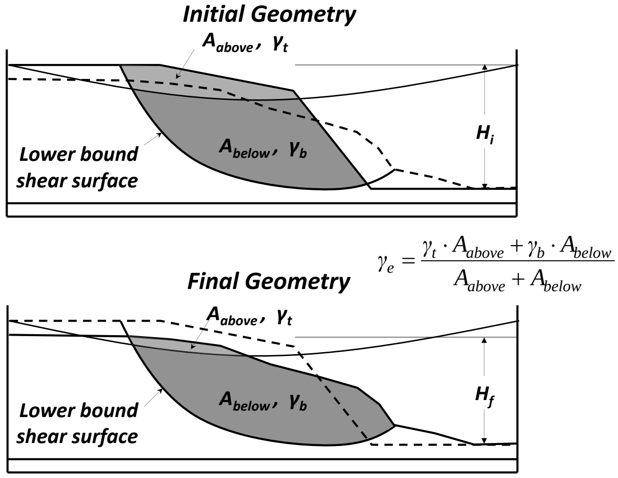

Fig. 4 Computation of equivalent unit weight for initial and final geometry

Table 2 Material properties of soils used in the study

Properties	San Francisco Bay Mud (SFBM)	Yolo Loam (YL)	Reference
LL (%)	88	29	Measured
PI (%)	50	10	Measured
Permeability coefficient, k (cm/s)	1.73×10^{-8} (at w=106%)	1.82×10^{-7} (at w=37%)	Measured from ICL consolidation test
Effective stress friction angle, ϕ	32.5-35		Bonaparte and Mitchell (1979)
Undrained strength ratio, S_u/p'	0.31-0.32 (Vane)		Bonaparte and Mitchell (1979)

Note, w = water content, p' = mean effective stress

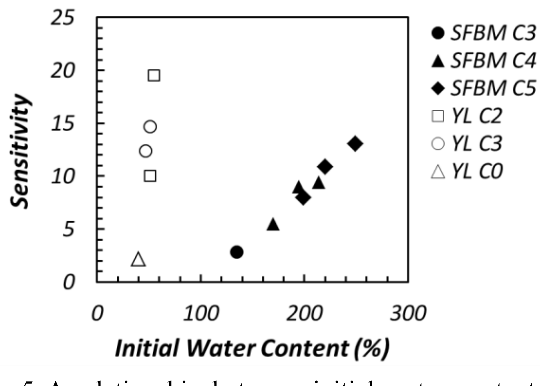

Fig. 5 A relationship between initial water content and mean sensitivity for centrifuge models

2.3.1 Sensitivity and water content

Researchers have shown that there is a reasonable correlation between sensitivity (S_t) and water content (Chew *et al.* 2004, Cotecchia and Chandler 2000, Park *et al.* 2010).

It is expected that S_t increases with initial water content. If initial water content increases, then LI (liquidity index defined as w–PL / PI, where w is water content, PL is plastic limit, and PI is plasticity index) also increases indicating an increase of S_t. Fig. 5 supports the same trend indicated in the previous studies. The trend between S_t and initial water content is positive cross-correlation (Javankhoshdel and Bathurst 2015). Note that high plasticity SFBM has a broader band of water content with lesser sensitivity change than Yolo Loam. S_t varies significantly within a narrow zone of water content change for Yolo Loam.

2.3.2 Shear strengths

In this study, shear strength was measured by hand-held vane shear device (shown in Park *et al*. 2014). Sensitivity (S_t) is therefore defined as peak vane shear strength (S_u) divided by remolded vane shear strength (S_{ur}).

The vane shear device has a diameter of 19 or 33 mm, and height of 28.5 or 49.5 mm depending on the stiffness of soil. For the peak shear strength measurement, rotation rate was 360°/min. For remoulded strength measurement, the rotation was made at 6 rpm after rapid 5 revolutions.

During centrifuge testing, S_u by vane shear is not constant at all depths as a result of centrifuge spinning. Thus, S_u and S_{ur} in the model container box were typically taken either at upper part of crest area (~ 25 mm from the surface) or at lower part of crest area (~ 25 mm from the base of clay layer) after stopping centrifuge (Park and Kutter 2015). Note that ρ_{us} and ρ_{sf} are the settlement from upslope and slope front displacement gauges during centrifuge spinning (Fig. 1).

From measurements of shear strengths at these two locations, all models indicated the dependence of shear strength on the depth of clay mass. At greater depth, shear strength was always higher than that of the upper layer. Since the soil was normally consolidated in the tests, the shear strength profile was regarded to be linearly proportional to depth. For the computation of instability factor at failure for analysis later, representative vane shear strength was taken as the mean value of the two (as seen in the Table 3).

During centrifuge spinning, static consolidation was measured through linear potentiometers. Consolidation during spinning can be an important factor to increase soil strength. Consolidation also contributes to the gradient of shear strength depending on the depth. Although consolidation settlement is not significant, a moderate amount of consolidation (about 2-3% of H for YL C2 models and 4% of H for SFBM C5 model) was observed from sensor measurement and visual inspection as shown in Table 3.

Because shear strengths were measured after the test instead of in-flight, there can be different effects on the interpretation of the strength. During the construction of the centrifuge model, vane shear strength was separately measured from the unconsolidated vane sample which had been sealed and cured apart from the centrifuge model. Shear strengths of the unconsolidated sample were lower than those measured in the centrifuge model after the test. It might be because of partial drying out of centrifuge models by spin-up and static consolidation at 50 G.

Table 3 Shear strength and its variation with depth, consolidation settlement (ρ_c) measured from the upslope potentiometer and strength gradient of centrifuge models

Test ID	S_u	S_{ur}	S_u (upper)	S_u (lower)	S_u gradient	S_u (top)	S_u (bottom)	ρ_c	e_o
	kPa	kPa	kPa	kPa	kPa/m	kPa	kPa		
DSP1	16.3	2.0			2.10	1.94	25.5		
DSP2	5.9	0.5			0.55	3.24	7.09		
DSP3	4.0	1.4			0.08	3.8	4.4		
DSP4	84.2	6.8	48	120	20.5	28.4	139.9	0 %H at 50 G	1.3
DSP5	62.5	4.3			11.3	22.8	102.2		
DSP6	3.3	0.4			0.44	1.7	4.9		
DSP7	4.8	0.5			0.36	3.5	6.0		
DSP8	9.8	1.8	7.3	12.3	1.11	5.9	13.7	4.6 %H at 40 G	4.13
DSP9	18.0	1.8	12.6	23.4	2.4	9.6	26.4	2.2 %H at 50 G	1.25
DSP10	4.5	0.4	4.0	4.9	0.2	3.7	5.2	3.7 %H at 50 G	5.33
DSP11	12.2	0.6	7.3	17.1	2.2	4.6	19.8	2.9 %H at 50 G	1.46
DSP12	10.9	5.1			2.67	0.63	19.3		

Note, S_u = representative undrained peak shear strength, S_{ur} = representative remolded shear strength, S_u (upper) = measured strength at 25 mm from the surface after centrifuge test, S_u (lower) = measured strength at 25 mm from the base after centrifuge test, S_u gradient = shear strength increase per unit depth based on the measured values between S_u (upper) and S_u (lower) assuming linear proportion with depth, S_u (top) and S_u (bottom) = shear strengths on the surface of crest and on the bottom of clay layer extrapolated from vane shear measurements, ρ_c = measured consolidation settlement at the upslope potentiometer during static spinning of centrifuge, and e_o is the initial void ratio.

2.3.3 Unit weight of soil

Unit weights of SFBM and YL are different depending on initial water content and thus affects strength gradient. In order to create centrifuge model with appropriate strength (e.g., about 2-40 kPa) and failure level (e.g., 5 to 10% settlement) in this study, it is recommended to use 2 to 5% of cement and 1.5 to 2.5 times the liquid limit of initial water content. With this recipe, addition of a significant amount of water results in a reduction of the unit weight as seen in the Fig. 6(a). The trend of the negative cross-correlation is fairly consistent. The reason of the negative correlation would be derived from the relation between water content (w), void ratio (e), and unit weight (γ). If w increases, e increases too. Relatively, specific gravity (Gs) and unit weight of water (γ_w) remain constant. Thus, the equation of saturated unit weight, $\gamma_{sat} = [(Gs + e) / (1 + e)] * \gamma_w$, yields decreased unit weight because of much higher variation of denominator, (1 + e).

Interestingly, unit weight change (about 1.5 kN/m^3) for YL occurs over a relatively narrower range of initial water content than SFBM. From the Fig. 6(a), YL has higher unit weight (16.3 to 17.8 kN/m^3) than SFBM (11.9 to 13.7 kN/m^3). As shown in the Fig. 6(b), higher unit weight of YL generates relatively higher strength gradient in terms of

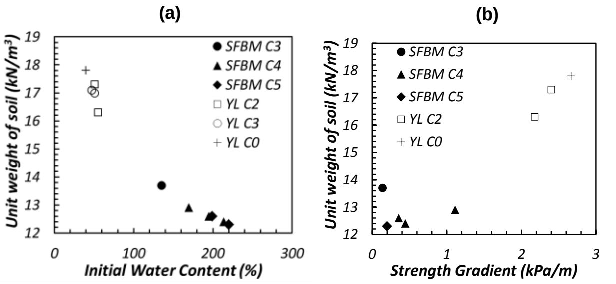

Fig. 6 The relationship of unit weight of soil and (a) initial water content and (b) strength gradient (S_u gradient) in centrifuge modelling

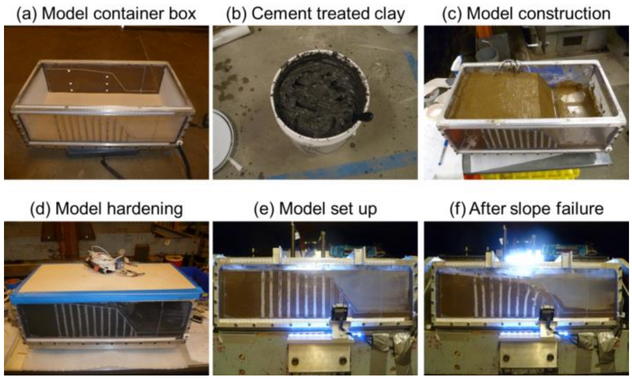

Fig. 7 Centrifuge model construction

depth, which can cause less extended deformed area for cement-treated YL than for cement-treated SFBM.

2.4 Model construction

Model construction procedure is described in Park and Kutter (2015). A visual procedure of model construction is shown in the Fig. 7. Depending on the spinning schedule and the desired target strength, one to seven days of curing were allowed. De-ionized water was filled up to the desired water level in front of the slope. After putting the model on the arm, every sensor cable was connected to right channels according to the instrumentation configuration.

2.5 Instrumentation

Instrumentation layout is composed of multiple accelerometers (to measure shaking induced acceleration at each point), pore pressure transducers (to measure pore pressure response within the soil due to static or dynamic event), and linear potentiometers (to measure vertical settlement on the surface of model slopes). All sensors were properly calibrated before use. Accelerometers (made by PCB Piezotronics) embedded into clay layer were waterproofed. The capacity range of accelerometers was 50 to 200 g. A base accelerometer was horizontally installed on the base of the model container so that the achieved motion can be compared to desired input motion. The capacity range of pore pressure transducers (made by DRUCK) was 50 to 100 psi. Measured pore pressure was compared with computed hydrostatic pore pressures on the basis of curved shape water table considering effective radius of centrifuge.

Table 4 Reference input motions for dynamic centrifuge modeling except DSP 8

Earthquake	Sequence*	Applied Test	Year	M	Station	Symbol	a_{peak} (g)	f_n (Hz)	D_n(s)
Loma Prieta	(1)	DSP5, 6	1989	6.9	Yerba Buena Island	LP-YBI	0.029	1.7	3
Loma Prieta	1	DSP7,9-12	1989	6.9	Monterey City Hall 090	LP-MCH	0.063	3.0	3
Northridge	2 (2)	DSP5-7, 9-12	1994	6.7	El Monte, LA	NOR-EM	0.158	2.0	11
San Fernando	3	DSP7, 9-12	1971	6.6	Castaic Old Ridge Route	SanF-CORR	0.324	3.0	15
ChiChi	4 (3)	DSP5-7, 9-12	1999	7.6	TCU-W	TCU	0.444	1.6	30
Chile	5 (4)	DSP5-7, 9-12	2010	8.8	Concepcion San Pedro	CCSP	0.605	4.5	152

Note, M = moment magnitude of earthquake, a_{peak} = peak acceleration, f_n = predominant frequency, D_n = duration of earthquake motion. *Sequence numbers in the brackets indicates the order of shaking for DSP 5 and DSP 6 test. Other dynamic tests except DSP 8 adopted the 5 successive motions as shown.

Table 5 Input motions and its characteristics for DSP 8 test

Earthquake	Symbol	Number of shaking	a_{peak} (g)	f_n (Hz)	Number of cycles
Sine Wave	SINE	9	0.20-0.45	1.2	5
		1	0.29	1.6	5
		3	0.42-0.62	2.0	5

Note that the number of shaking indicates the number of repetitive series of shaking with sinusoidal wave having particular a_{peak}, f_p, and the number of cycles.

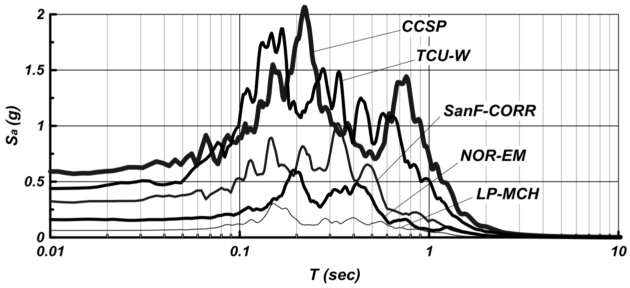

Fig. 8 Acceleration response spectra (ARS) of input motions for centrifuge earthquake simulation. Note, S_a = spectral acceleration, T = period

Two linear potentiometers (made by BEI Duncan) installed measured static consolidation as well as shaking induced deformation time histories on the surface. A typical instrumentation layout is shown in the Fig. 1.

2.6 Input motions

For dynamic centrifuge modeling (as shown in Table 1), five different earthquake motions were chosen (Table 4). Fig. 8 displays acceleration response spectra (ARS) of each motion. Two dynamic tests (DSP 5 and 6) used four motions. Exceptionally, DSP 8 used different sinusoidal motions to check the performance of two-way sliding block approach which is shown later. For DSP 8, a total of 13 sine waves were applied with different amplitudes and frequencies as summarized in the Table 5. All the other five dynamic tests used five motions (Table 4).

In this research, multiple shakings were successively applied for each dynamic model. The order of application of

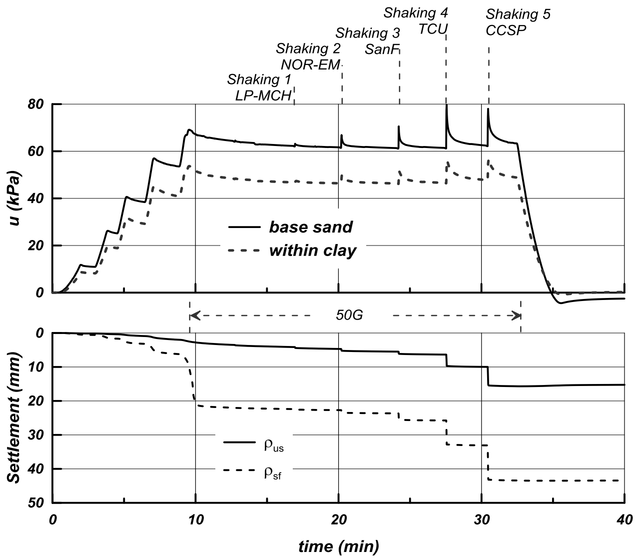

Fig. 9 An example plot of pore pressure and displacement responses for the DSP11 (YL C2W55T3) model

the input motions is shown in Table 4. Earthquake motions were applied starting from small earthquake motions to the biggest one, the CCSP motion. Though the sequence of shaking is a little different from each group of dynamic centrifuge test, all tests except DSP 8 had the same two final input motions–TCU and CCSP. Sequence is important in tests with successive motion as slope response can be affected with increased slip due to a geometrical effect as the slope flattens (Al-Defae *et al*. 2013). Later, there was some permanent deformation due to each shaking as expected and each stepping displacement was tracked using measurement of linear potentiometers.

For application of input motions, 4th order band-pass filter were applied to avoid any harmful resonance of centrifuge machine itself. The corner frequencies were 0.8 Hz and 100 Hz. The natural frequency of centrifuge machine was estimated to be about 20 Hz at 50 g, which is 0.4 Hz at 1g condition. Note that there were limitations of the shaker controller. Initially, the amplification factor required to match the desired target motion with the measured base motions was unknown. Hence, some trials were required to command input motions. There were sometimes several shakings of different amplification factors even with the same motion to match the target PGA (peak acceleration measured on the ground).

2.7 Test features

For static tests (DSP1 to 4), the main goal was to determine the G-level at failure. During the centrifuge spinning, consolidation and dissipation rate of excess pore pressure was observed. For dynamic tests (see Table 1), during or after each input motion, excess pore pressure change was measured and each shaking was applied after dissipation of excess pore pressure which was generated by previous shaking event. Dissipation of excess pore pressure was checked by observing pore pressure reaching down to the hydrostatic pore pressure after each shaking. Fig. 9 shows an example plot of pore pressure and displacement responses for the DSP11 (YL C2W55T3) model including static and each dynamic shaking induced excess pore pressure generation and dissipation with respect to the time.

Table 6 G-level or PGA to cause settlements of 2%, 5%, and 10% of slope height (H)

Test code	G-level or PGA that caused a certain degree of settlements					
	2% H		5% H		10% H	
	ρ_{us}	ρ_{sf}	ρ_{us}	ρ_{sf}	ρ_{us}	ρ_{sf}
DSP3 SFBM C3W135T9	24	14	32	16	46	46
DSP8 SFBM C4W170T7	41	35	50	40	Sine (±0.49 g,1.2 Hz)	45
DSP7 SFBM C4W195T2	36	38	43	46	50	NOR-EM (0.108 g)
DSP6 SFBM C4W214C2	30	28	37	35	46	49
DSP1 SFBM C5W199T6	>>50	>>50				
DSP2 SFBM C5W249T6	>>50	>>50				
DSP10 SFBM C5W220T1	50	50	TCU (0.543 g)	50	N/A	TCU (0.543 g)
DSP12 YL C0W40	21	21	50	39	SanF (0.424g)	43
DSP9 YL C2W51T3	LP-MCH (0.065 g)	46	CCSP (0.392 g)	50	N/A	50
DSP11 YL C2W55T3	50	35	TCU (0.559 g)	49	CCSP (0.556 g)	50
DSP4 YL C3W47T5	N/A	N/A	>>50	N/A	N/A	N/A
DSP5 YL C3W51T4	N/A	N/A	>>50	N/A	N/A	N/A

Note that static G-level during dynamic shaking was 50G

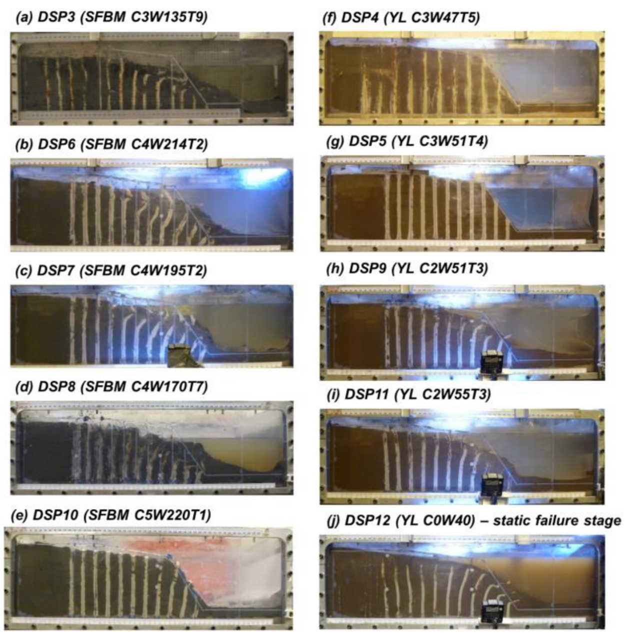

Fig. 10 Deformed shape for centrifuge model clay slopes

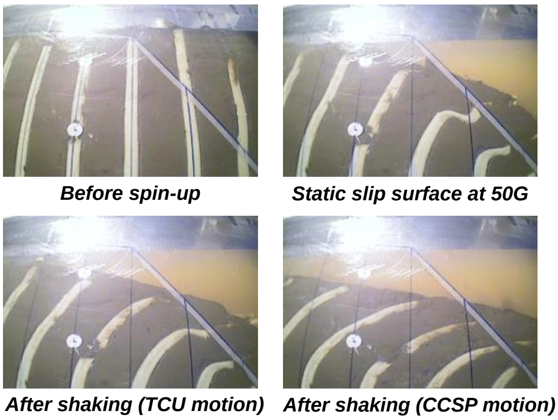

Fig. 11 Snapshots taken from side wall CCD camera for DSP12 model

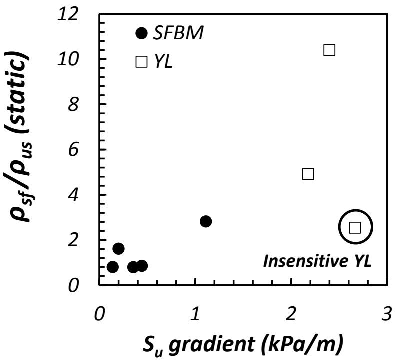

Fig. 12 Settlement ratio (at the slope front / at the upslope) and gradient of shear strength gaining depending on depth

3. Results

Based on careful observation and data analysis, the cement mix ratio and the initial water content have significant effect on failure level. For SFBM models, DSP10 indicated no static failure and very limited dynamic failure. DSP6, DSP7, and DSP8 models displayed static deformation (at close to 50 G), and also dynamic failure. DSP3 model shows extensive static failure at the low G-level. For Yolo Loam, the DSP4 and DSP5 models has no failure even under 0.6 g of strong shaking. The DSP9 and DSP11 models presented no static failure, but dynamic failure at strong shaking events.

Earthquakes with higher peak acceleration (> 0.4 g) and long duration like TCU-W (30 s) and CCSP-E motions (150 s) clearly generates significant deformation. PGA less than 0.3 g does not generate significant deformation for cemented SFBM and YL. From DSP8 test (SFBM C4W170T7), multiple sine waves make more extensive deformation than real earthquakes though PGA remains similar.

The Yolo Loam model without cement treatment shows the difference of static and dynamic failure (Fig. 11). The Fig. 11 is the snapshots taken at each stage of sequential event for DSP12. A distinctive static slip surface is developed near the steep slope. However, dynamic failure occurs in a widely diffused shear surfaces. The potential factors that may affect the thickness of shear surfaces are shown in Park and Kutter (2015). Note should be taken that the dynamic deformation must be partially affected by pre-defined static deformation because of multiple loading stages. As seen in Fig. 11, the static failure lead to a flatter slope around distinct shear surface and this pre-existing shear surface would also remold adjacent areas. This influence of multiple loading sequences should be acknowledged for detail interpretation though static failure surface is observed in a distinct and shallow manner.

One of the reasons for diffused shear surfaces during dynamic loading might be two-way sliding. Input motions have a variety of positive and negative momentary accelerations. Thus, when the soil slope is subjected to multiple loading in both directions, corresponding deformation is the combination of multiple back and forth movements. As a net deformation at the end of shaking, widely distributed shear surfaces are observed.

A comparison can be made between strength gradient per depth and the settlement ratio of slope front and upslope area. As seen in Fig. 12, settlement at the slope front increases as the gradient of shear strength increases for cement-treated clays, except uncemented YL (DSP12). In Fig. 12, higher S_u gradient in kPa/m is expected to be shallower slip surface. Higher ρ_{sf} / ρ_{us} represents that the deformed area is expected to be narrower toward the slope front. Uncemented YL shows relatively higher S_u gradient but similar level of ρ_{sf} / ρ_{us} as cement treated sensitive SFBM. Comparing uncemented YL and the other two YLmodels, Fig. 12 supports that sensitive soil typically tends to deform in a more localized manner toward the slope front.

From the observations, it has been shown that sensitivity can be incorporated into reconstituted soils used in physical modelling. Sensitivities up to 20 were obtained in this study (Table 1).

4. Analysis and discussion

4.1 Slope failure and variation of instability factor

Slope instability depends on the definition of failure reflected by the strain level of concern. Thus, it is useful to clearly define the term, 'slope failure' in this study. Two settlement transducers were used on the surface of upslope and slope front area (Fig. 1). Failure was deemed to occur when the settlement reaches 5% of the total slope height on the upslope area.

Because γ_e and H gradually change as deformation proceeds, instability factor actually changes too. Thus, it is meaningful to correlate instability factors before and after static loading as shown in Table 7. Fig. 13 shows how instability factor (N_I) at 50G (which is the target G-level) varies depending on the reduction of unit weight and slope height as deformation proceeds. In Fig. 13, note that the initial and final N_I at 50G means N_I before any deformation at 50G and N_I after final deformation at 50G respectively, computed by $\gamma_e H / S_u$ using Eqs. (4), (5), and H_i, H_f. In Fig. 13, final N_I is equal or less than initial N_I at 50G. It is useful to check if the Taylor's traditional criterion is still valid to

Table 7 Change of equivalent unit weight and slope height depending on deformation of slope

Material	γ_{ei}	γ_{ef}	H_i	H_f	$\gamma_{e,5\%}$	$\gamma_{e,10\%}$	$H_{5\%}$	$H_{10\%}$	$N_{I,5\%}$	$N_{I,10\%}$
	kN/m^3	kN/m^3	mm	mm	kN/m^3	kN/m^3	mm	mm		
DSP3	9.8	7.2	120	99.4	8.8	7.9	112.4	104.9	8.0	9.6
DSP8	3.6	5.7	120	85						
DSP7	5.9	4.3	120	100.5	5.5	5.2	115.6	111.1	5.7	6.0
DSP6	4.6	3.1	120	96.7	4.2	3.9	114.4	108.9	5.4	5.9
DSP1	3.0	3.0	100	100						
DSP2	2.7	2.7	120	120						
DSP10	3.9	3.1	120	103.8						
DSP12	9.3	8.2	120	72	9.1	8.9	111.4	102.8	4.7	
DSP9	9.9	8.2	120	98						
DSP11	8.3	6.8	120	98						
DSP4	8.2	8.2	120	120						
DSP5	8.1	8.1	120	120						

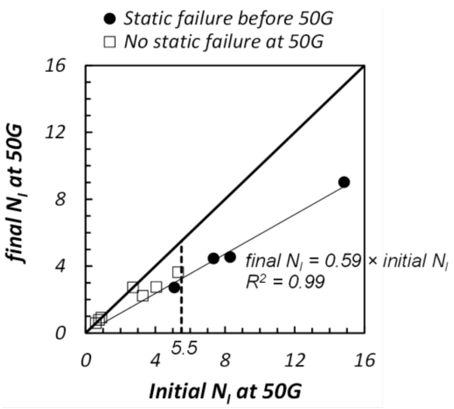

Fig. 13 Comparison of instability factor (N_I) at 50 G for initial and final geometry

quickly judge slope stability of cement treated clay. As seen in Fig. 13, a borderline N_I for initial geometry is about 5 to 5.5 to differentiate static failure and no static failure. N_I using equivalent unit weight to cause a failure is in reasonable agreement shown in the Taylor's chart ($N_I \sim 5.5$). Another way to predict slope instability in this testing scheme is to relate static failure to the ratio of the initial and final instability factors once final geometry is known. As seen in Fig. 13, static failure is observed when the final N_I is about equal or less than 0.59 times initial N_I.

4.2 Limit equilibrium analysis

Limit equilibrium analysis was applied for the evaluation of slope stability. The SLOPE/W program (version 2007, Geo-Slope International Ltd.) was used for limit equilibrium analysis. All calculations of factor of safety (FS) used the General Limit Equilibrium (GLE) method (Fredlund and Krahn 1977). The GLE method accommodates a wide range of different interslice force functions satisfying both moment and force equilibrium. The non-circular optimized slip surface was applied in the analysis. For the pseudo-static approach, seismic force is applied at the centroid of each slice. Yield acceleration coefficients (k_y) were obtained by finding the k_y value for soil slope to be unstable (i.e., FS = 1.0).

For material strength envelope in the limit equilibrium analysis, a linear variation of strength with depth was assumed and hence shear strengths were linearly extrapolated from the middle of the top vane shear test to the soil surface (as seen in the Table 8). In SLOPE/W, strength as a function of depth was therefore adopted. For cement-treated clay, extrapolated strength at the crest had a certain non-zero value, which might be caused by a true cohesion by cementation effect, effective overconsolidation associated with cementation and consolidation due to cement hydration, and possibly negative pore water pressure above the water table.

In each case, the location of critical slip surface was searched for to produce minimum FS. Note that the location of critical slip surface is dependent on soil strength. For purely frictional case, the minimum FS always tends to be surface raveling. Meanwhile, the critical slip surface for undrained strength model like this study tends to extend as deep as possible. In this study, the computed critical slip surface to yield minimum FS was compared to the observed major slip surface from the deformed shape of deformation columns after dissection (e.g., Fig. 14). Fig. 14 displays an example regarding computed critical slip surface and observed major slip surface / lower bound shear surface. A red hatched zone is the safety map which shows the region of FS between FS_{min} (minimum factor of safety) and 1.5 times FS_{min}. It is seen that the computed critical slip surface and the observed slip surface are in a reasonable similarity to each other.

Based on the static and pseudo-static limit equilibrium analysis, the results of analyses are summarized in the Table 8.

Based on the Table 8, when computed static factor of safety (FS) for forward sliding is below 1.0 (DSP3, 6, 7, and 12), values of G-level or PGA to cause 5%H settlement at the upslope area are less than 50 G, which means static failure. To the contrary, models with FS > 1.0 (DSP1, 2, 4, 5, 9, and 11) shows there were no static failure at 50 G. It is observed that limit equilibrium analysis using peak strength as a function of depth mostly works fine to evaluate the stability of cement-treated clay slopes. There are a couple exceptions (e.g., DSP8 and DSP10) in that limit equilibrium analysis does not account for the effect of cement mixing ratio, which can be related to the degree of cementation.

DSP10 was stable at 50 G in spite of FS below 1 from limit equilibrium analysis due to potentially higher cement mixing ratio. The reason is not clear at this time but cement mixing ratio may affect the shear strength in other ways that are not measured by the vane shear. The fact is that SFBM C5 models (DSP 1, 2, 10) showed much higher static resistance than SFBM C4 models (DSP 6, 7, 8) which failed at much less G-level. Since the only variable to make a difference between SFBM C5 and C4 models is the cement mixing ratio and it is believed to be contributable. The reason why S_u for DSP10 is less than that of the other higher water content with the same cement mixing ratio (i.e., DSP 2; SFBM C5W249T6) is that the former curing period at the earlier stage of hardening was much less than the latter. This difference of S_u is believed to affect the

Table 8 Limit equilibrium analysis to compute undrained factor of safety for centrifuge models

Model	Label	γ	Static FS at 50G		G-level or PGA	K_{yp}	K_{yn}	K_{yn}/K_{yp}
			Forward sliding	Back-ward sliding	at $\rho_{5\%H\text{-}US}$	Forward sliding	Back-ward sliding	
		kN/m^3						
DSP3	SFBM C3W135T9	13.7	0.411		32 G			
DSP8	SFBM C4W170T7	12.9	2.162	5.260	50 G			
DSP7	SFBM C4W195T2	12.6	0.673	1.521	43 G			
DSP6	SFBM C4W214C2	12.4	0.447	0.943	37 G			
DSP1	SFBM C5W199T6	12.6	2.867		>> 50 G			
DSP2	SFBM C5W249T6	11.9	1.859		>> 50 G			
DSP10	SFBM C5W220T1	12.3	0.685	1.826	TCU (50G + 0.543 g)			
DSP12	Uncemented YL W40	17.8	0.649	1.341	50 G			
DSP9	YL C2W51T3	17.3	1.597	4.246	CCSP (50G + 0.392 g)	0.182	0.384	2.1
DSP11	YL C2W55T3	16.3	1.085	2.585	TCU (50G + 0.559 g)	0.032	0.235	7.3
DSP4	YL C3W47T5	17.1	8.055		>> 50G			
DSP5	YL C3W51T4	17.0	4.600	11.44	>> 50G			

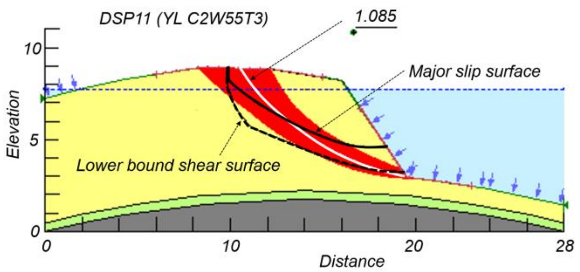

Fig. 14 Result of limit equilibrium analysis for DSP11 (YL C2W55T3) model

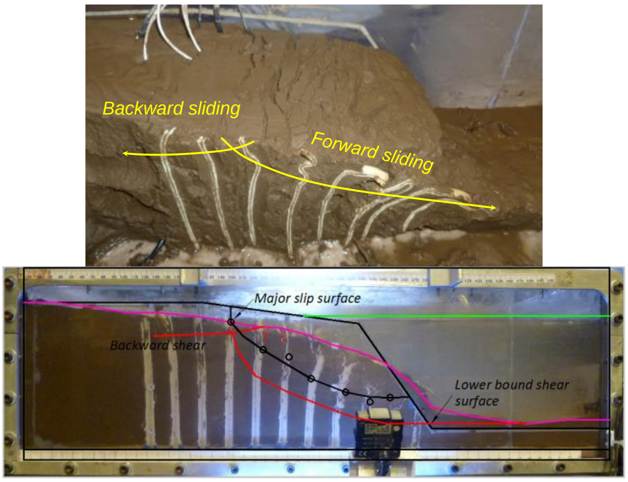

Fig. 14 Result of limit equilibrium analysis for DSP11 (YL C2W55T3) model

computed FS from limit equilibrium analyses.

DSP8 was expected to be stable from the limit equilibrium analysis, but it failed at 50 G. A part of reason would be pre-applied multiple small shakings before centrifuge spinning for calibration of the newly installed controller.

In Table 8, for the comparison of DSP9 and DSP11, DSP9 is more stable at 50 G (static FS = 1.597) and yet seems to only withstand a 0.39 g shaking whereas DSP11 having less S_u is only marginally stable at 50 G (static FS = 1.085) and yet seems to sustain 0.55 g of shaking. However, according to the sequence of multiple shaking event applied, in fact, DSP9 model showed no dynamic failure at TCU event (achieved a_{peak} = 0.55 g), which was preceded CCSP event (achieved a_{peak} = 0.392 g). Note that the duration of CCSP motion is much longer than TCU motion. DSP11 model showed a failure at TCU event (achieved a_{peak} = 0.56 g) before CCSP shaking motion.

One note is that the slope stability analysis shows a toe circle as being critical while the observed result shows the failure surface exiting along the slope. According to the Taylor's chart, a toe circle failure occurs if the slope angle is greater than 54°. Thus, the toe circle failure is expected in this study considering the steep slope angle of 55°, as the limit equilibrium analysis shows. But in many cases of failure, the observed failure surface was within the slope. There might be various reasons such as the possibility of strength gradient change during centrifuge spinning with the effect of consolidation settlement, and the effect of radial G-field. The combination of settlement and confining pressure dependent stress field during spinning could potentially cause stiffening and increase the strength gradient a little, which led to relatively shallower failure surface. Another reason could be that the radial G-field effect created a different failure surface location between the linear model geometry with a curved water table and the curved virtual prototype geometry with a linear water table.

As a result of limit equilibrium analysis, curved geometry gives a little less factor of safety (about 0.1 difference in the factor of safety) than straight geometry. Hence, in this study, the curved geometry was used for analysis because of more accurate evaluation of instability and possible backward sliding by earthquake motions. This two-way sliding is important to compute permanent displacement because one-way sliding block analysis never catches the up and down fluctuation of slope deformation. Two-way sliding behavior might be a better way to predict slope displacement. To do so, positive and negative yield acceleration coefficients can be obtained from pseudo-static analysis. From Table 8, as expected, backward sliding has much higher yield coefficient. Factor of safety is also higher than forward sliding.

Two-way sliding is also supported by observation of deformed shape as shown in Fig. 15. Fig. 15 shows the cross-sections after dynamic shaking. The figure provides a proof of backward shearing though the dominant failure surface towards the toe of the slope. Visual inspection of vertical deformation noodles provided an evidence of curved geometry due to the radial G-field effect. Despite the existence of a steep slope to the right, the left side of the model displays the backward shear surface near the top portion due to radial G-field effect during centrifuge acceleration. As seen in Fig. 14, the use of transformed virtual prototype geometry was useful for slope stability analysis because it enabled more accurate evaluation of instability, and possible backward sliding, of slopes by earthquake motions.

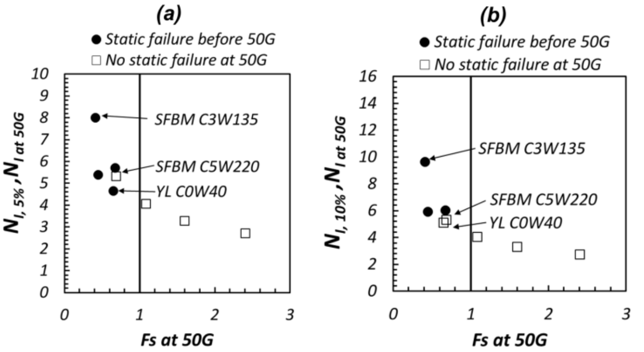

Fig. 16 A relationship of observed N_I and computed FS from limit equilibrium analysis

Forward and backward sliding may relate to diffused shear surfaces. Because dynamic shaking leads to multiple back and forth movements, more distributed shear surfaces are observed than static cases as a net deformation at the end of shaking.

In this study, yield accelerations were computed from limit equilibrium analysis for DSP9 and DSP11. Conceptually, if acceleration at a certain time step is greater than the yield acceleration or the relative velocity of the soil mass is greater than zero, permanent displacement occurs. When we think about two-way sliding, k_{yn}-yield acceleration toward backward (denoted as negative, 'n'), and k_{yp}-yield acceleration toward forward (denoted as positive, 'p'), physically k_{yp} is never equal to k_{yn} except for level ground. For a slope, the magnitude of k_{yp} is less than or equal to k_{yn}. Therefore, the net two-way sliding displacement should be always equal or less than the one-way sliding displacement. In this study, a term, 'forward sliding' means rightward movement toward the toe, and 'backward sliding' represents leftward movement toward the crest. Positive and negative yield acceleration coefficients were obtained by finding the seismic coefficient, k_y value for soil slope to be unstable (i.e., FS = 1.0). Since SLOPE/W software does not find k_y automatically, it was necessary to iterate to obtain the value that just makes FS = 1.0.

4.3 Static stability of slopes

Fig. 16(a) shows the relationship of observed instability factor to cause 5% settlement and computed factor of safety at 50 G from limit equilibrium analysis. Note that N_I was computed at 5% settlement of slope height for statically failed cases and was calculated at 50 G for no static failure. According to the Talyor's chart, the instability number to cause a slope failure should be about 5.5.

When failure is defined as 5% settlement in the upslope area, observed instability number to cause failure is about 5. At the cases of FS less than 1, we would expect static failure. The result is in good agreement except DSP10. For FS greater than 1 at 50 G, the observed result is in good agreement.

Fig. 16(b) is the same type of plot to address N_I at 10% settlement of slope height. As seen in the Fig. 16(b), overall instability factors increased for static failure cases. Computed FS is matched with observed one reasonably, but there are two exceptions-DSP10 and DSP12. The insensitive model, DSP12, shows 5% settlement at 50 G, but no 10% settlement for static loading. Depending on different strain level, different stability can be obtained. DSP10 model is relatively stable because of higher cement mix ratio (than 2 to 3% mixed ones) in spite of higher initial water content.

One particular outlier in the Fig. 16(b) is the DSP3 model. N_I at 10% settlement (= 9.6) is much higher than the expected value (= 5.5) at failure. Considering low S_t (= 3), 3% cement mixing to SFBM can be close to insensitive material. As shown in the DSP12 model, insensitive clay might be easier to reach relatively low deformation (e.g., 5% settlement) than high sensitive clays, but more difficult to reach large deformation (e.g., 10% settlement) because of the ductile stress-strain relationship. As a result, G-level to cause 10% settlement should be larger and thus N_I at 10% settlement as a failure criterion might be much higher.

5. Conclusions

Sensitive clays are soils that lose a large portion of their strength during remolding. As a part of efforts to understand the static and dynamic behavior of sensitive clay slopes, instability and deformation of centrifuge models were studied for artificially prepared sensitive clay slopes. In order to make sensitive clay slopes, the recipe suggested by Park *et al.* (2015) was used. A total of 12 centrifuge test results for the cement-treated and untreated clay slopes were analyzed. Analytical approach using instability factor (N_I; $\gamma H/S_u$), pseudo-static limit equilibrium analysis was performed to check their applicability. The followings highlight important findings.

• Physical modelling using weakly cement-treated clay slopes shown in Park *et al.* (2014) can effectively replicate strain softening clay behavior in terms of repeatability of strength and sensitivity. Sensitivities up to 20 (DSP11; YLC2W55T3) were obtained in this study. Physical modelling using weakly cement-treated clay slope is proved to be an effective tool to study strain softening clay slope stability in terms of sensitivity and shear strengths.

• Instability factor using equivalent unit weight (γ_e) to cause a failure is in reasonable agreement with 5.5 shown in the Taylor's chart with some exceptions relating cement ratio and sensitivity. Static instability factor (N_I) and limit equilibrium analysis using peak strength as a function of depth were reasonably applicable to evaluate the stability of cement-treated artificially sensitive clay slopes.

• Based on the observation after slope deformation, two-way sliding behavior might be a more reasonable approach to compute realistic permanent displacement induced by dynamic shaking for cement treated clay slopes. Also, two-way sliding may relate to diffused shear surfaces based on the observation of deformed shape after failure. Dynamic shaking leads to multiple back and forth movements. As a net deformation at the end of shaking, widely distributed shear surfaces are observed with less deformation than static cases.

• Radial G-field effect was an important factor for the computation of critical clip surface location when both rotation direction and longitudinal direction of model container coincide with each other. Transformed curved geometry considering radial G-field was required to accurately account for observed backward sliding and the location of major slip surface.

For future studies, a probabilistic analysis can be a good research subject to make this work more interesting. It is also interesting to perform finite element or finite difference analysis for the deformation and stress-strain analysis.

Acknowledgements

Centrifuge modelling in this paper was performed under the Shared Use program at NEES@UCD. Centrifuge tests were supported by NSF Grant 0530151 and NEES@UC Davis. The author wants to express sincere gratitude to the guidance of Professor Bruce Kutter throughout tests and valuable technical discussions. The author also appreciates Professor Jason DeJong and Dr. Dan Wilson for their sincere help during centrifuge tests.

References

Al-Defae, A.H., Caucis, K. and Knappett, J.A. (2013), "Aftershocks and the whole-life seismic performance of granular slopes", *Géotechnique*, **63**(14), 1230.

Andersson-Sköld, Y., Torrance, J.K., Lind, B., Oden, K., Stevens, R.L. and Rankka, K. (2005), "Quick clay-A case study of chemical perspective in Southwest Sweden", *Eng. Geol.*, **82**(2), 107-118.

Azizian, A. and Popescu, R. (2005), "Finite element simulation of seismically induced retrogressive failure of submarine slopes", *Can. Geotech. J.*, **42**(6), 1532-1547.

Baker, R., Shukha, R., Operstein, V. and Frydman, S. (2006), "Stability charts for pseudo-static slope stability analysis", *Soil Dyn. Earthq. Eng.*, **26**(9), 813-823.

Chew, S.H., Kamruzzaman, A.H.M. and Lee, F.H. (2004), "Physicochemical and engineering behavior of cement treated clay", *J. Geotech. Geoenviron. Eng.*, **130**(7), 696-706.

Cotecchia, F. and Chandler, R.J. (2000), "A general framework for the mechanical behaviour of clays", *Géotechnique*, **50**(4), 431-447.

Couture, R. (2011), *Introduction-National Technical Guidelines and Best Practices on Landslides*, Open File 6765, Geological Survey of Canada.

Crawford, C.B. (1968), "Quick clays of eastern Canada", *Eng. Geol.*, **2**(4), 239-265.

Demers, D., Robitaille, D., Locat, P. and Potvin, J. (2014), *Inventory of Large Landslides in Sensitive Clay in the Province of Quebec, Canada: Preliminary Analysis*, in *Landslides in Sensitive Clays*, Springer, 77-89.

Dey, R., Hawlader, B., Phillips, R. and Soga, K. (2016a), "Numerical modeling of combined effects of upward and downward propagation of shear bands on stability of slopes with sensitive clay", *Int. J. Numer. Anal. Meth. Geomech.*, **40**(15), 2076-2099.

Dey, R., Hawlader, B., Phillips, R. and Soga, K. (2016b), "Numerical modeling of submarine landslides with sensitive clay layers", *Géotechnique*, **66**(6), 454-468.

Duncan, J.M. and Wright, S.G. (2005), *Soil Strength and Slope Stability*, John Wiley & Sons, Inc.

Fredlund, D.G. and Krahn, J. (1977), "Comparison of slope stability methods of analysis", *Can. Geotech. J.*, **14**(3), 429-439.

Geertsema, M. and Torrance, J.K. (2005), "Quick clay from the Mink Creek landslide near terrace, British Columbia: Geotechnical properties, mineralogy, and geochemistry", *Can. Geotech. J.*, **42**(3), 907-918.

Geological Survey of Canada (2010), May 10, 2010 Landslide at St. Jude, Quebec, <http://gsc.nrcan.gc.ca/landslides/stjude_e.php>.

GEO-SLOPE International Ltd. (2010), *Stability Modeling with SLOPE/W 2007 Version*.

Gibson, R.E. and Morgenstern, N. (1962), "A note on the stability of cuttings in normally consolidated clays", *Géotechnique*, **12**(3), 212-216.

Holtz, R.D. and Kovacs, W.D. (1981), *An Introduction to Geotechnical Engineering*, Prentice-Hall, Englewood Cliffs, New Jersey, U.S.A.

Garnier, J., Gaudin, C., Springman, S.M., Culligan, P.J., Goodings, D., Konig, D., Kutter, B., Phillips, R., Randolph, M.F. and Thorel, L. (2007), "Catalogue of scaling laws and similitude questions in geotechnical centrifuge modeling", *Int. J. Phys. Modell. Geotech.*, **7**(3), 1-23.

Janbu, N. (1968), "Slope stability computations, soil mechanics and foundation engineering report", The Technical University of Norway, Trondheim, Norway.

Javankhoshdel, S. and Bathurst, R.J. (2015), "Influence of cross correlation between soil parameters on probability of failure of simple cohesive and c-ϕ slopes", *Can. Geotech. J.*, **53**(5), 839-853.

Javankhoshdel, S. and Bathurst, R.J. (2014), "Simplified probabilistic slope stability design charts for cohesive and cohesive-frictional (c-ϕ) soils", *Can. Geotech. J.*, **51**(9), 1033-1045.

Legget, R.F. and LaSalle, P. (1978), "Soil studies at Shipshaw, Quebec: 1941 and 1969", *Can. Geotech. J.*, **15**(4), 556-564.

L'Heureux, J.S., Locat, A., Leroueil, S., Demers, D. and Locat, J. (2014), "Landslides in sensitive clays -from geosciences to risk management", *Landslides Sensitive Clays Adv. Nat. Technol. Hazards Res.*, **36**, 1-12.

Locat, P., Demers, D., Robitaille, D., Fournier, T., Noël, F., Leroueil, S., Locat, A. and Lefebvre, G. (2012), "The Saint-Jude landslide of May 10, 2010, Québec, Canada", *Proceedings of the 11th International and 2nd North American Symposium on Landslides*, Banff, Alberta, Canada, June.

Longva, O., Janbu, N., Blikra, L.H. and Boe, R. (2003), "The 1996 Finneidfjord slide; seafloor failure and slide dynamics", *Proceedings of the EGS-AGU-EUG Joint Assembly Meeting*, Nice, France, April.

Park, D.S. (2014), "The effect of radial G-field on the centrifuge modeling", *Proceedings of the 8th International Conference on Physical Modelling in Geotechnics (ICPMG2014)*, Perth, Australia, January.

Park, D.S. and Kutter, B.L. (2016), "Sensitive bounding surface constitutive model for structured clay", *Int. J. Numer. Anal. Meth. Geomech.*, **40**(14), 1968-1987.

Park, D.S. and Kutter, B.L. (2015), "Static and seismic stability of sensitive clay slopes", *Soil Dyn. Earthq. Eng.*, **79**, 118-129.

Park, D.S., Kutter, B.L. and DeJong, J.T. (2014), "Effects of thixotropy and cement content on the sensitivity of soft remolded clay", *J. Geotech. Geoenviron. Eng.*, **141**(2), 04014095.

Park, D.S., Kutter, B.L. and DeJong, J. (2010), "Centrifuge modeling of a sensitive clay slope for simulation of strain softening", *Proceedings of the 7th International Conference on Physical Modelling in Geotechniques*, International Society for Soil Mechanics and Geotechnical Engineering, Zurich, Switzerland, July.

Quinn, P.E., Diederichs, M.S., Rowe, R.K. and Hutchinson, D.J. (2011), "A new model for large landslides in sensitive clay using a fracture mechanics approach", *Can. Geotech. J.*, **48**(8), 1151-1162.

Rezania, M., Taiebat, M. and Poletti, E. (2016), "A viscoplastic SANICLAY model for natural soft soils", *Comput. Geotech.*, **73**, 128-141.

Seed, H.B. and Wilson, S.D. (1967), "The Turnagain Heights landslide, Anchorage, Alaska", *J. Soil Mech. Found. Div.*, **93**(SM4), 325-353.

Spencer, E. (1967), "A method of analysis of stability of embankments assuming parallel inter-slice forces", *Géotechnique*, **17**(1), 11-26.

Steward, T., Sivakugan, N., Shukla, S. and Das, B. (2011), "Taylor's slope stability charts revisited", *Int. J. Geomech.*, **11**(4), 348-352.

Talesnick, M. and Baker, R. (1984), "Comparison of observed and calculated slip surface in slope stability calculations", *Can. Geotech. J.*, **21**(4), 713-719.

Tappin, D.R., Watts, P. and Matsumoto, T. (2003), *Architecture and Failure Mechanism of the Offshore Slump Responsible for the 1998 Papua New Guinea Tsunami* in *Submarine Mass Movements and Their Consequences*, Kluwer, The Netherlands, 383-389.

Taylor, D.W. (1937), "Stability of earth slopes", *J. Boston Soc. Civ. Eng.*, **24**(4), 197-246.

Taylor, D.W. (1948), *Fundamentals of Soil Mechanics*, John Wiley and Sons, New York, U.S.A.

Thakur, V. and Nordal, S. (2005), "Rate dependent elasto plastic deformation of shear bands in sensitive clays", *Elec. J. Geotech. Eng.*, **10**.

Updike, R.G., Olsen, H.W. and Schmoll, H.R. (1988), *Geologic and Geotechnical Conditions Adjacent to the Turnagain Heights landslide, Anchorage, Alaska*, Department of the Interior, U.S. Geological Survey, Denver, Colorado, U.S.A.

USGS. (2015), Landslide Events, Landslide Hazards Program, U.S. Geological Survey, <http://landslides.usgs.gov/recent>.

Wilson, D.W., Kutter, B.L. and Boulanger, R.W. (2010), "NEES @ UC Davis", *Proceedings of the 7th International Conference on Physical Modelling in Geotechnics*, Zurich, Switzerland, July.

GC